Mechanism-Based Inactivation of Cytochromes by Furan Epoxide: Unraveling the Molecular Mechanism

ARTICLE *in* INORGANIC CHEMISTRY · NOVEMBER 2013

Impact Factor: 4.76 · DOI: 10.1021/ic401907k · Source: PubMed

3 AUTHORS:

Nikhil Taxak
Evalueserve
18 PUBLICATIONS **108** CITATIONS
SEE PROFILE

Sourav Kalra
Central University of Punjab
5 PUBLICATIONS **7** CITATIONS
SEE PROFILE

Prasad V Bharatam
National Institute of Pharmaceutical Educatio…
244 PUBLICATIONS **2,321** CITATIONS
SEE PROFILE

Inorganic Chemistry

Article

pubs.acs.org/IC

Mechanism-Based Inactivation of Cytochromes by Furan Epoxide: Unraveling the Molecular Mechanism

Nikhil Taxak, Sourav Kalra, and Prasad V. Bharatam*

Department of Medicinal Chemistry, National Institute of Pharmaceutical Education and Research (NIPER), Sector 67, S. A. S. Nagar (Mohali), 160 062 Punjab, India

Supporting Information

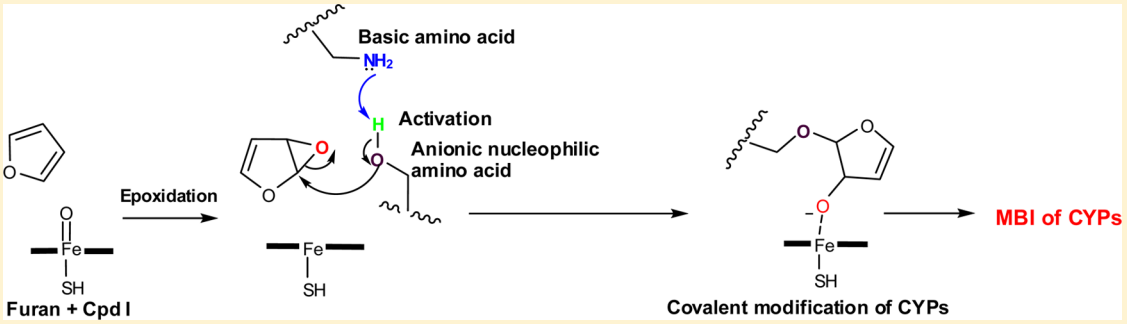

ABSTRACT: Drugs carrying an unsaturated C═C center (such as furans) form reactive epoxide metabolites and cause irreversible mechanism-based inactivation (MBI) of cytochrome P450 (CYP450) activity, through covalent modification of amino acid residues. Though this reaction is confirmed to take place in the active site of CYPs, the details of the reactions of furan (epoxidation and epoxide ring opening), the conditions under which MBI may occur, the residues involved, the importance of the heme center, etc. have yet to be explored. A density functional theory (DFT) study was carried out (i) to elucidate the reaction pathways for the generation of furan epoxide metabolite from furan ring by the model oxidant **Cpd I** (iron(IV)-oxo heme-porphine radical cation, to mimic the catalytic domain of CYPs) and (ii) to explore different reactions of the furan epoxide metabolite. The energy profiles of the competitive pathways and the conditions facilitating MBI of CYPs by the reactive epoxide metabolite are reported. The rate-determining step for the overall metabolic pathway leading to MBI was observed to be the initial epoxidation, requiring ∼12 kcal/mol under the enzymatic conditions. The covalent adducts (inactivator complexes) are highly stable (∼−46 to −70 kcal/mol) and may be formed due to the reaction between furan epoxide and nucleophilic amino acid residues such as serine/threonine, preferably after initial activation by basic amino acids.

INTRODUCTION

Epoxides are very important versatile intermediates in organic and biosynthetic pathways and undergo a plethora of reactions such as nucleophilic substitution reactions (S_N1 and S_N2) and hydrolysis reactions, giving rise to a variety of products.[1−7] Several scientific groups have reported the chemistry of epoxidation reactions and highlighted the role of the epoxide ring-opening process in synthetic reactions. Many experimental studies on the epoxidation reaction and epoxide ring opening under bioinorganic conditions are available in the literature.[8−15] Nam et al. studied the epoxidation of olefins by hydrogen peroxide (HOOH) catalyzed by iron(III) porphyrin complexes in protic and aprotic solvents.[8,9] Song et al. studied the influence of reaction conditions on the competitive reactions, olefin epoxidation, alkane hydroxylation, and C═C epoxidation, by in situ generated oxoiron(IV) porphyrin π-cation radicals.[10]

A few quantum chemical studies have also been reported on the epoxidation reaction by metal complexes, such as metalloporphyrins containing iron, chromium, and manganese, metal cyclam complexes, peroxo complexes of Cr(VI), Mo(VI), and W(VI), etc.[16−19] The epoxidation reaction has also been studied in the presence of model oxidants mimicking the catalytic domain of cytochromes P450 (CYP450).[20−23] Shaik et al. studied alkene epoxidation with **Cpd I** (iron(IV)-oxo heme porphine radical cation with SH^- as the axial ligand) and showed a preference for the epoxidation of *cis*-alkenes over *trans*-alkenes.[20] Kumar et al. reported the fundamental factors responsible for the epoxidation in substrates such as ethene, cyclohexadiene, 1-butene, styrene, etc.[21] de Visser et al. reported a comparative study of the epoxidation reaction and the allylic hydroxylation reaction of propene with **Cpd I**.[22] Lonsdale et al. reported a comparative study of epoxidation and hydroxylation of cyclohexene and propene, using hybrid quantum mechanical/molecular mechanical (QM/MM) methods.[23]

Epoxides are also present naturally in biological systems such as in enzyme vitamin K epoxide reductase, which participates in the blood coagulation process.[24] Epoxide hydrolases are being

Received: July 23, 2013
Published: November 15, 2013

   dx.doi.org/10.1021/ic401907k | Inorg. Chem. 2013, 52, 13496−13508

Scheme 1. Metabolic Pathway of Furan Ring via (i) Epoxidation by Cpd I and (ii) Ring Opening by Nucleophilic Amino Acid Residues

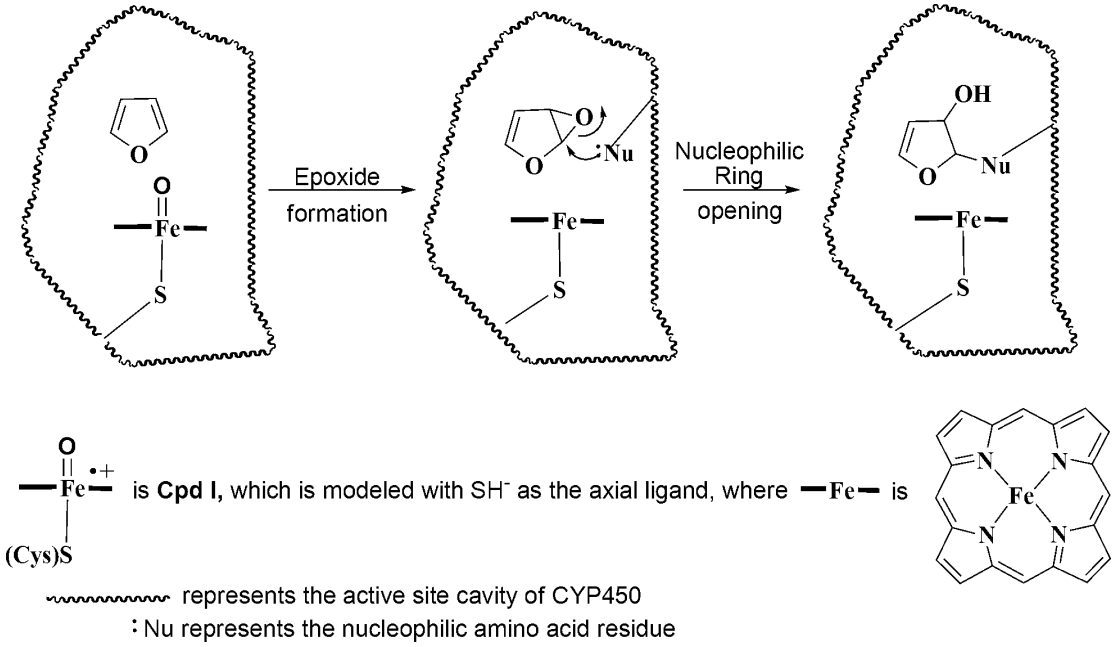

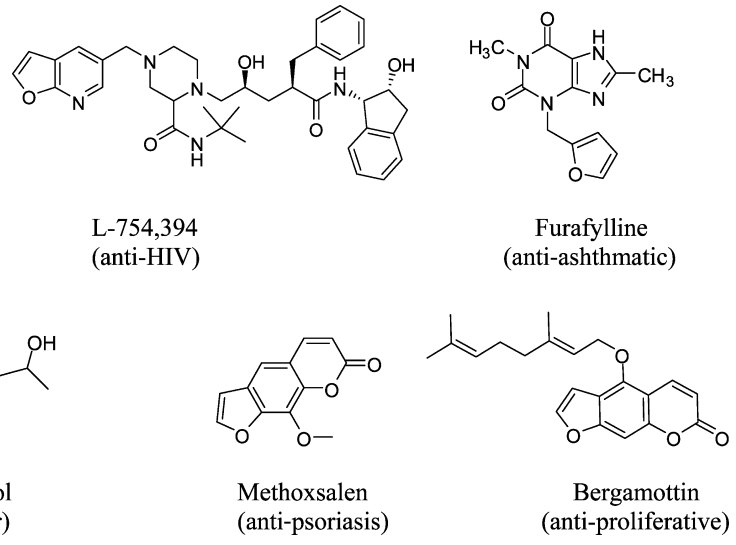

Figure 1. Structures of drugs and natural compounds containing furan ring leading to MBI of CYPs via epoxidation.

utilized as a therapeutic target for the control of blood pressure, acute inflammation, and cardiovascular diseases.[25]

In biological systems, epoxidation is a key metabolic step, catalyzed by CYPs, for several drugs containing functional groups such as alkenes, furan, thiophene, phenyl, pyridine, etc. Sometimes, this epoxide metabolite being highly reactive and electrophilic leads to the covalent modification of active site nucleophilic amino acid residues in CYPs (Scheme 1).[26−38] This phenomenon is known as irreversible Mechanism-Based Inactivation (MBI) of CYPs, which leads to drug−drug interactions and associated drug toxicity.[39] The epoxide metabolite is termed as the mechanism-based inactivator which interferes with the catalytic cycle of CYPs and distorts its structure via covalent adduct formation (inactivator complex). This inactivation being irreversible underlies its concern in drug metabolism.

MBI by the reactive epoxide metabolite is mostly observed in drugs containing furan ring, thiophene, and an alkene group.[39] Drugs containing thiophene moiety undergo competitive S-oxidation reaction, along with epoxidation.[39] Alkene group containing drugs lead to MBI via alkylation of the heme-prosthetic group.[39c,f,h,i] On the other hand, drugs and natural compounds containing a furan ring (Figure 1) lead to MBI of CYPs via the reactive epoxide metabolite, as evidenced by reported experimental studies.[26−38]

Sesardic et al. reported the inhibitory potential of furafylline (1,8-dimethyl-3-(2′-furfuryl)methylxanthine) toward CYP1A2.[26] Kunze and Trager carried out a detailed study on the isoform selective MBI of CYP1A2 by furafylline.[27] Chiba et al. studied the mechanism for MBI of CYP3A4 by the HIV protease inhibitor L-754,394, which was proposed to occur via epoxide ring opening by nucleophilic amino acid residues.[28]

dx.doi.org/10.1021/ic401907k | Inorg. Chem. 2013, 52, 13496−13508

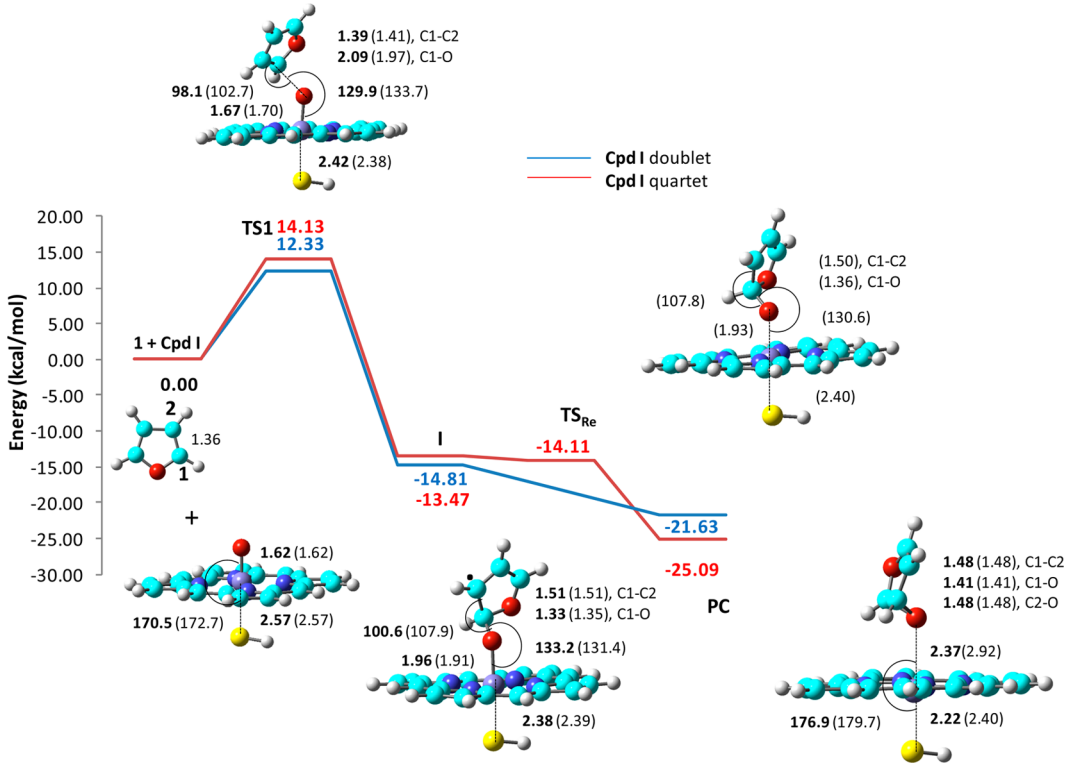

Figure 2. Reaction profile and optimized geometries for furan epoxidation by **Cpd I** (doublet and quartet spin states). Energy values are given in kcal/mol, bond distances in Å, and bond angles in deg. Values written in boldface are on the doublet spin state of **Cpd I**, and those within parentheses are on the quartet spin state of **Cpd I**. Color code: red, oxygen; sky blue, carbon; white, hydrogen; blue, nitrogen; gray, iron; yellow, sulfur.

Lightning et al. reported that the enzyme inactivation by L-754,394 was not reversible upon extensive dialysis.[29] Koenigs et al. reported the CYP2A6 irreversible inactivation by methoxsalen, via the epoxide metabolite.[30]

Tinel et al. reported the suicidal inhibition of CYP activity by methoxsalen via the loss of spectrally observable heme.[31] Schmiedlin-Ren et al. discussed the MBI of CYPs by the coumarin derivative corandrin, similar to methoxsalen.[32] Alvarez-Diez et al. reported time and concentration-dependent irreversible inactivation of more than 80% of CYP3A4 by 4-ipomeanol.[33] Edwards et al. reported the inhibitory potential of 6′,7′-dihydroxybergamottin and its parent compound, bergamottin.[34] He et al. and Girennavar et al. reported the inactivation potential of bergamottin toward CYP3A4 via the modification of the apoCYP450 in the active site of the enzyme.[35,36] Guo et al. discussed the CYP3A4 inhibitory potential of furanocoumarin bergapten (5-methoxypsoralen), present in grapefruit peel oil and some plant foods such as parsley, parsnips, and celery.[37] Ueng et al. have reported the MBI of CYP2A6 by chalepensin in human liver microsomes and proposed the involvement of epoxide metabolite in this inactivation.[38]

Thus, the reported experimental studies point to the limitations of furan ring containing drugs and natural compounds and have highlighted the formation of covalent adducts of epoxide metabolite with amino acid residues. Though a few of the above studies proposed possible mechanisms, the molecular level details for the epoxidation and nucleophilic ring opening leading to MBI are still elusive; the conditions favorable for MBI and the residues involved have not been reported in the literature. Several lead compounds with furan rings are in the early phase of testing and clinical trials, and the furan epoxide metabolite is acting as a perpetrator for potential adverse reactions and MBI. Hence, it becomes imperative to study these details to avoid this phenomenon in the early phase of drug discovery. The in-depth analysis and accurate prediction of MBI requires an understanding of the reaction mechanisms responsible for the formation of these RMs and their reactivity. This can be achieved by employing quantum chemical methods, such as in the reported studies to address MBI by RMs such as nitroso, carbenes, alkynes, and hydrazines.[40,41]

Quantum chemical studies reported in this article explore (i) the mechanism of epoxidation of furan (model substrate) and (ii) the reaction pathways available for the reactive epoxide metabolite. Thus, understanding the mechanistic details associated with the reactive epoxide metabolite formation due to the furan ring would aid in focusing the efforts of computational, medicinal, and metabolism scientists toward metabolically safe compounds with a furan ring or any other unsaturated moiety, at earlier stages of drug discovery and development.

COMPUTATIONAL METHODOLOGY

DFT (density functional theory)[42] was utilized to understand the process of epoxidation and epoxide ring opening of furan and elucidate the metabolic reaction pathway leading to covalent modification of CYPs. The Gaussian03 suite[43] of programs was used to carry out all the geometry optimizations on the metabolic path of the furan ring and estimate the absolute energies. The B3LYP hybrid density functional was used for geometry optimizations and frequency calculations in CYP related studies, where the LanL2DZ basis set[44] was used on iron and the 6-31+G(d) basis set[45] was used on all the

dx.doi.org/10.1021/ic401907k | Inorg. Chem. 2013, 52, 13496−13508

Scheme 2. Proposed Pathways for the Biotransformation of Furan Ring to Various Intermediates[a]

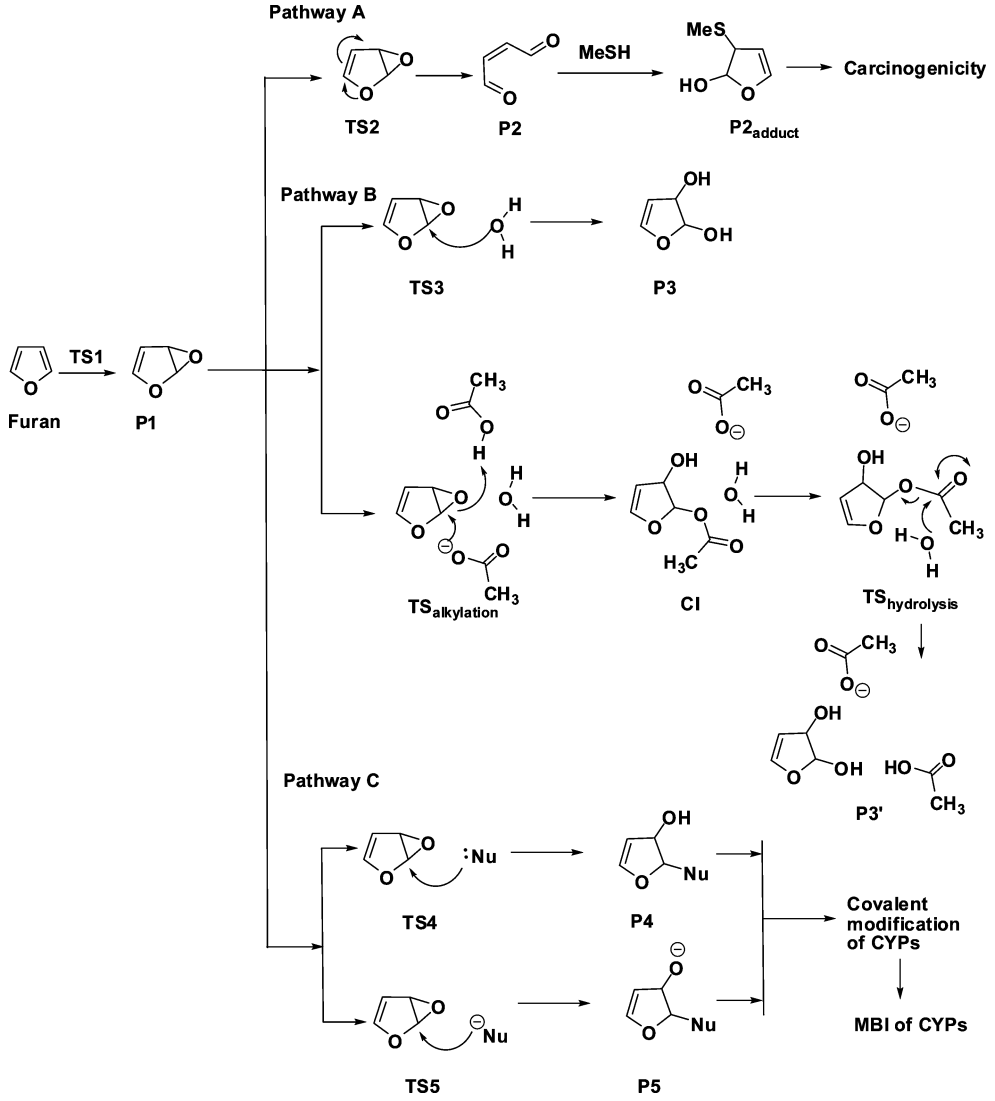

[a]Abbreviations: **TS1**, transition state for **Cpd I** catalyzed furan epoxidation; **P1**, furan epoxide; , transition state for furan ring cleavage; **P2**, *cis*-2-butene-1,4-dial; $\mathbf{P2_{adduct}}$, covalent adduct with MeSH; **TS3**, transition state for direct hydrolysis by water; **P3**, furan vicinal diol; $\mathbf{TS_{alkylation}}$, transition state for acid-assisted ring opening; **CI**, covalent intermediate; $\mathbf{TS_{hydrolysis}}$, transition state for ester hydrolysis; **P3′**, complex of furan diol with carboxylate anion and carboxylic acid; **TS4**, transition state for epoxide ring opening by neutral nucleophile; **P4**, nucleophilic adduct of furan epoxide; **TS5**, transition state for epoxide ring opening by anionic nucleophile; **P5**, anionic nucleophilic adduct of furan epoxide.

remaining atoms; the basis set is denoted as BS1. Frequency calculations were also performed with the same basis set to characterize the stationary points to minima and transition states to first-order saddle points with one imaginary frequency vibrational mode.[46] Zero-point energy (ZPE) values were obtained after incorporating a scaling factor of 0.9806.[47] **Cpd I** was used as the model oxidant to mimic CYPs, which are iron(IV)-oxo radical cations with heme-porphine and SH^- as the axial ligand.[48] The axial ligand represents the cysteinate linkage by which the heme is linked to the protein in CYPs. This model has been reported in several metabolism-related studies on CYP-catalyzed reactions and provides reasonable energy estimates.[21−23,48] The mechanistic studies were explored on both the doublet and quartet spin states of **Cpd I**. Single-point energy calculations were carried out using the TZVP triple-ζ basis set for iron[49] and the 6-311+G(d) basis set for all the remaining atoms; this basis set is denoted as BS2. Solvent-phase calculations were performed using the integral equation formalism variant of the polarizable continuum model (IEFPCM)[50] with implicit solvent chlorobenzene (ε = 5.7) to mimic the dielectric constant in the active site of cytochrome enzyme; this basis set is denoted as BS3. Previous studies of our group and other groups have showed that the combination of these basis sets gives reliable geometries and energetics.[21−23,40,41,48] Spin densities and charge distribution were obtained using Mulliken population analysis and the NBO[51] method, respectively. The Atoms in Molecules (AIM)[52] method was employed to identify the intramolecular hydrogen bonding interaction in *cis*-2-butene-1,4-dial, using the AIM2000 software package. The bond critical point and ring critical points were determined using the AIM method. Electrophilicity and nucleophilicity parameters were calculated using standard equations mentioned in the Supporting Information (S1).[53,54] The geometric parameters and energies discussed in this article are based on basis set BS3, unless otherwise specified. The structures of the intermediates, transition states, and products on the reaction pathways are elucidated and the potential energy profile of the reactions is traced.

RESULTS AND DISCUSSION

In this article, the results are presented in two sections: (i) furan epoxidation using **Cpd I** and (ii) plausible reactions of the furan epoxide metabolite.

dx.doi.org/10.1021/ic401907k | *Inorg. Chem.* 2013, 52, 13496−13508

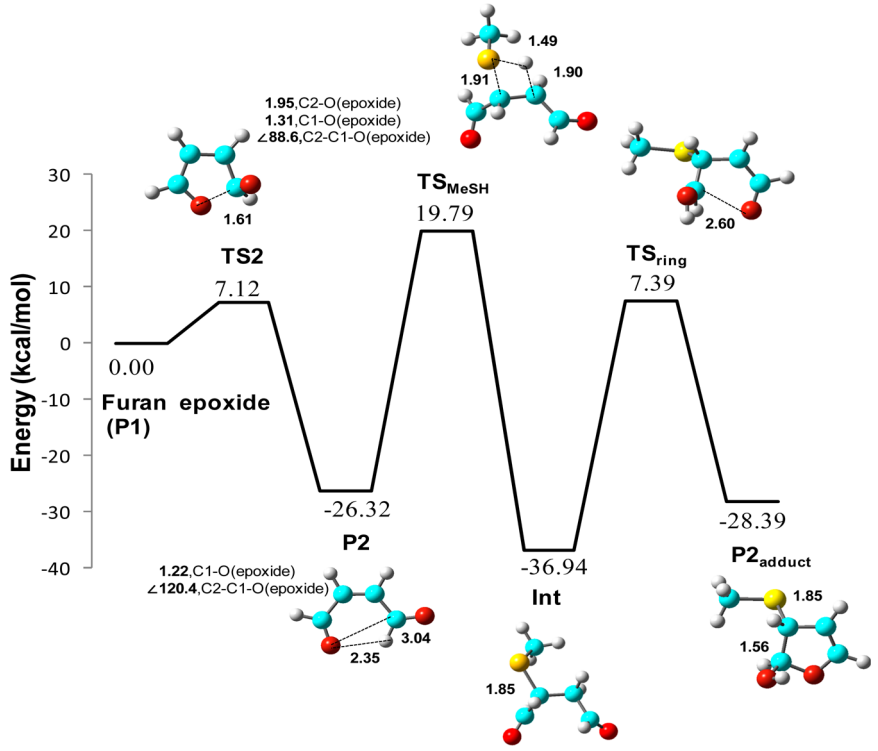

Figure 3. Potential energy surface and optimized structures for pathway A. All energy values are given in kcal/mol, bond distances in Å, and bond angles in deg. Color code: red, oxygen; sky blue, carbon; white, hydrogen; blue, nitrogen; gray, iron; yellow, sulfur.

Furan Epoxidation by Cpd I. Several studies have been reported on the epoxidation of a range of substrates such as ethene, propene, 1-butene, *trans*-2-butene, cyclohexadiene, styrene, etc. using **Cpd I** as the model oxidant.[21−23] The mechanism of epoxidation has been reported to involve two steps, initial C−O bond formation via C═C bond activation and the rebound step leading to the generation of the epoxide product.[21−23] The epoxidation reaction of furan was studied on both the doublet and quartet spin states of **Cpd I** using the BS3 basis set, incorporating implicit solvent (chlorobenzene) effects and zero point vibrational corrections.

Figure 2 shows the whole reaction pathway for the furan epoxidation starting from the isolated reactants,[4,2] **Cpd I** and the model furan ring. The reaction mechanism involved (i) an initial C1═C2 activation (**TS1**) leading to the formation of the radical intermediate (**I**) with a C1−O bond, followed by (ii) ring closure generating the epoxide metabolite (**PC**, a complex of furan epoxide denoted as **P1** and heme-porphine; Figure 2). The estimated barriers are 12.33 and 14.13 kcal/mol on the doublet and quartet spin states of **Cpd I**. The corresponding barriers at the BS2 basis set were 8.80 (doublet) and 9.44 (quartet) kcal/mol, respectively, which are similar to reported barriers for the epoxidation of the substrates ethene (14.29 and 14.13 kcal/mol), propene (12.60 and 13.13 kcal/mol), 1-butene (13.52 and 11.06 kcal/mol), styrene (9.53 and 8.95 kcal/mol), 1,3-cyclohexadiene (9.42 and 7.90 kcal/mol), 1,4-cyclohexadiene (13.12 and 11.94 kcal/mol), etc.[21−23] Kumar et al. reported barriers of 9.1 and 17.3 kcal/mol for epoxidation of 1,3-cyclohexadiene and 1,4-cyclohexadiene with the BS3 basis set on the doublet spin state.[22] Kumar et al. reported an increase in activation barrier values for a majority of substrates with the BS3 basis set with the inclusion of implicit solvent conditions (ε = 5.7). This increase can be attributed to an enhanced localization exerted by the medium polarization effect of chlorobenzene solvent.[22] The spin density shifts more on the porphyrin ring, instead of the cysteine ligand. Thus, owing to the different behavior of **Cpd I** in the presence of the implicit solvent (external conditions), several scientific groups have characterized **Cpd I** as a chameleon species.[21−23] Owing to the smaller activation barrier on the doublet spin state at all the three basis sets used in the study, the rest of the discussion on the reaction mechanism has been limited to the doublet spin state of **Cpd I**.

The transition state **TS1** showed a marginal elongation of the C1−C2 bond (1.36 to 1.39 Å), while the C1- - -O(Fe) bond was observed to be 2.09 Å on the doublet spin surface of **Cpd I** (Figure 2). The Fe- - -O bond distance was observed to be marginally increased to 1.67 Å in **TS1** from 1.62 Å (**Cpd I**). This transition state was also characterized by Fe−O−C1 and O−C1−C2 bond angles of 129.9 and 98.1°, respectively, indicating a change in the orientation of furan to undergo oxygen insertion. **I** is the intermediate complex (ΔH = −14.81 kcal/mol), which was characterized by further elongation of the C1−C2 bond to 1.51 Å, giving it a significant single-bond character. The C1−O bond distance was observed to be reduced to 1.33 Å, while the Fe−O distance increased to 1.96 Å, as shown in Figure 2. This step is followed by subsequent ring closure to generate the furan epoxide product complex (**PC**). This step involved a smaller rebound barrier of 0.64 kcal/mol on the quartet spin state (**TS$_{Re}$**) as shown in Figure 2, whereas it occurred via a barrierless reaction on the doublet spin state. **PC** was characterized by a weak Fe- - -O electrostatic interaction (2.37 Å), and was stable by −21.63 kcal/mol on the doublet spin potential energy (PE) profile.

PC (global electrophilicity index ω = 2.48 eV) was found to be more electrophilic than **I** (ω = 0.99 eV); hence, it can undergo ring-opening reactions preferably. The epoxide oxygen

dx.doi.org/10.1021/ic401907k | *Inorg. Chem.* 2013, 52, 13496−13508

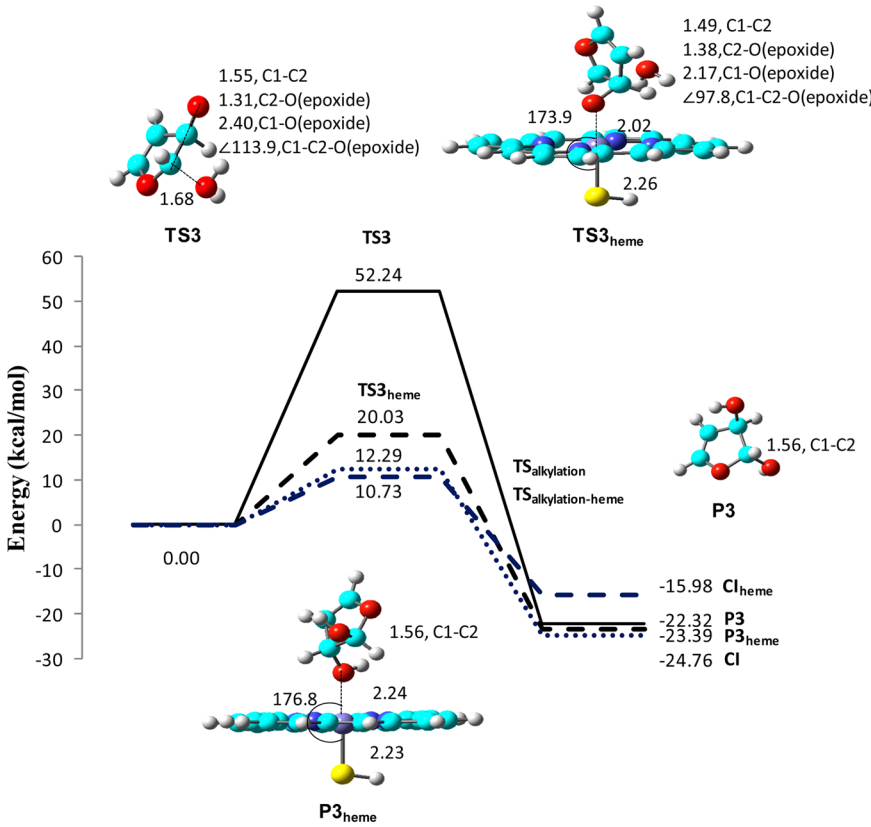

Figure 4. Potential energy surface on pathway B: direct hydrolysis (black line); heme-porphine catalyzed hydrolysis (dotted black line); acid assisted hydrolysis (blue dots); heme-dependent acid assisted hydrolysis (dotted blue line). Energy values are given in kcal/mol. Optimized geometries on the direct hydrolysis pathway are also shown. Bond distances are given in Å and bond angles in deg. Other optimized structures are shown in Figure 5. Color code: red, oxygen; sky blue, carbon; white, hydrogen; blue, nitrogen; gray, iron; yellow, sulfur.

was observed to be oriented directly above the heme-iron, with an Fe−O bond distance of 2.37 Å.

Reactions of Furan Epoxide Metabolite. Several scientific groups have proposed various consequences of the furan epoxide metabolite,[39,55] which can be categorized into three pathways as shown in Scheme 2. Pathway A involves furan ring cleavage leading to the formation of the electrophilic dialdehyde intermediate **P2** (eventually leading to $\mathbf{P2}_{\mathbf{adduct}}$), which is implicated in carcinogenicity.[39g,55] Pathway B involves the hydrolysis of the epoxide ring to yield the vicinal dihydrodiol metabolite (**P3**). It may also occur via the assistance of a carboxylic acid, similar to that observed in epoxide hydrolases,[56] to generate the complex of a diol metabolite (**P3′**). Pathway C involves epoxide ring opening by nucleophiles (**TS4**/**TS5**), leading to the generation of covalent adducts (**P4**/**P5**), which block the catalytic site, eventually leading to MBI of CYPs.[26−39] Pathway A does not involve the role of CYPs; pathway B may occur in CYPs depending on the presence of water molecules in the active site. On the other hand, pathway C is CYP-catalyzed and involves the crucial role of nucleophilic amino acid residues in the covalent modification of the enzyme.

Pathway A: Non-CYP-Catalyzed Furan Ring Cleavage. A few furan ring containing drugs undergo internal rearrangement after epoxidation, as shown in Scheme 2, to generate the electrophilic intermediate (**P2**).[55] This rearrangement involves the assistance of the lone pair of electrons on furanyl oxygen in the simultaneous ring opening of the epoxide. The electrophilic intermediate is *cis*-2-butene-1,4-dial, which undergoes nucleophilic addition reactions with glutathione (GSH), DNA nucleobases (2′-deoxyguanosine and 2′-deoxyadenosine), or amino acids such as *N*-acetylcysteine.[55] It has been reported that furan as such is inactive in the Ames assay for mutagenicity; however, the unsaturated dialdehyde metabolite is observed to be mutagenic in this assay.[56] The addition reactions to this dialdehyde metabolite subsequently give rise to mutagenic and carcinogenic adducts.

Figure 3 shows the energy profile on pathway A, where the rearrangement of **P1** occurs via **TS2** involving a barrier of 7.12 kcal/mol. **TS2** was characterized by an increase of the C1- - - O_{furan} distance to 1.61 Å from 1.36 Å in furan. Figure 3 shows the 3D structure of **TS2**, where the epoxide ring was observed to be partially broken, as indicated by the C2- - -O bond distance of 1.95 Å and C2−C1−O bond angle of 88.6°. **TS2** generates the stable dialdehyde intermediate **P2** (ΔH = −26.32 kcal/mol with respect to furan epoxide, **P1**). **P2** can undergo nucleophilic addition reaction with methanethiol (MeSH, a model nucleophile for glutathione) via $\mathbf{TS}_{\mathbf{MeSH}}$ (E_a = 19.79 kcal/mol) to form the highly stable **Int**, which after proton transfer and ring closure ($\mathbf{TS}_{\mathbf{ring}}$, E_a = 7.39 kcal/mol) forms the stable adduct $\mathbf{P2}_{\mathbf{adduct}}$ (ΔH = −28.39 kcal/mol). All attempts to locate the protonated intermediate connecting **Int** and $\mathbf{TS}_{\mathbf{ring}}$ did not yield any viable structure. Both barriers involved in the nucleophilic addition reaction with respect to **P1** were significantly higher (>40 kcal/mol), hence undermining the probability of a nucleophilic addition reaction to **P2** to form $\mathbf{P2}_{\mathbf{adduct}}$. Further on this pathway, **P2** and **Int** are sufficiently stable and no driving force for the formation of $\mathbf{P2}_{\mathbf{adduct}}$ can be

dx.doi.org/10.1021/ic401907k | *Inorg. Chem.* 2013, 52, 13496−13508

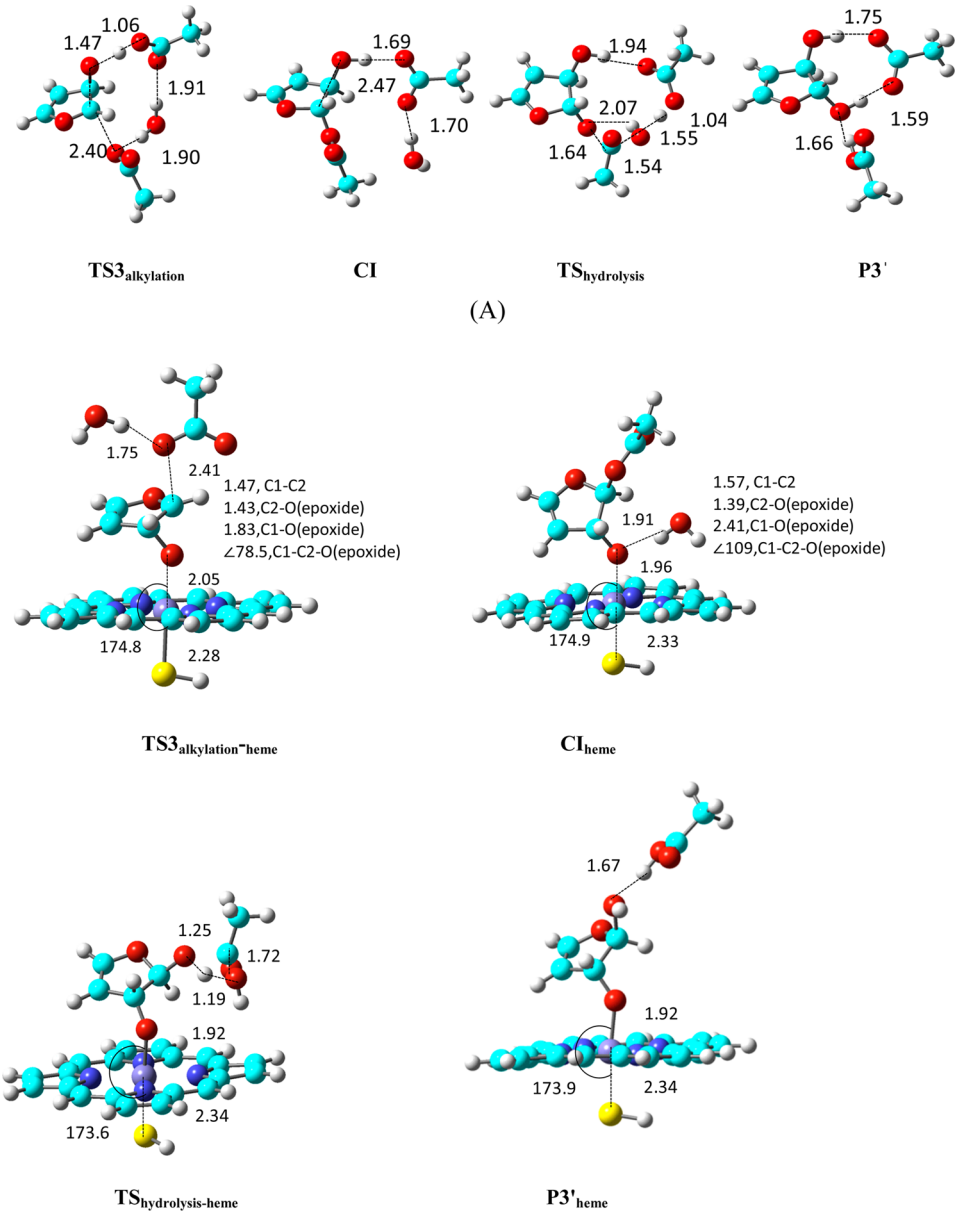

Figure 5. BS3 optimized geometries of species involved in acid-assisted hydrolysis of furan epoxide in (A) the absence of heme-porphine and (B) the presence of heme-porphine (doublet spin state of **Cpd I**). Bond distances are given in Å and bond angles in deg. Color code: red, oxygen; sky blue, carbon; white, hydrogen; blue, nitrogen; gray, iron; yellow, sulfur.

envisaged. **P2** was characterized by an intramolecular H-bonding interaction (C−H- - -O_{furan}, = 2.35 Å), supported by AIM analysis (Figure S1, Supporting Information).

Since **P2** is electrophilic in nature, similar to furan epoxide (**P1**), global and local electrophilicity indices were estimated for both intermediates (Table S2, Supporting Information). The global electrophilicity index (ω) indicates that **P2** (ω = 3.894 eV) is more electrophilic than **P1** (ω = 1.072 eV). In **P1**, the most electrophilic center is C1, whereas in **P2**, the most electrophilic center is C2 (Table S2, Supporting Information).

The rate-determining step on pathway A was observed to be nucleophilic addition to **P2**, as shown in Figure 3. Since the dial (**P2**) formation from **P1** has been reported in a few carcinogenicity experiments, it may be possible that the formation of **P2** occurs outside the active site cavity of CYPs. Moreover, the barriers for steps 2 and 3 in the process are too high for an enzymatic system; hence, it is unlikely that this process takes place in the enzyme. Inside the cavity of CYPs, heme center dependent pathways (pathways B and C) may prevail.

Pathway B: Hydrolysis by Water Molecule(S) In the Active Site Cavity of CYPs. Furan epoxide metabolite can undergo hydrolysis by nearby water molecule(s) in the active site cavity of CYPs.[39g] However, this possibility is generally small, owing to the hydrophobic character of active sites of CYPs (Figure S2, Supporting Information). This reaction results in the formation of vicinal diols (Scheme 2), which are generally nontoxic in nature. This reaction may occur via two mechanisms: (i) direct attack of the water molecule on the epoxide ring or (ii) a carboxylate ion and carboxylic acid assisted process (covalent

dx.doi.org/10.1021/ic401907k | Inorg. Chem. 2013, 52, 13496−13508

intermediate formation followed by hydrolysis), similar to the case for epoxide hydrolases.[57] Quantum chemical analysis was carried out to explore both possibilities, and this comparative study helped in identifying the catalytic role of the nucleophile (carboxylate ion) and the acid catalyst (carboxylic acid) in the ring opening.

(i). Direct Hydrolysis of Furan Epoxide by Water Molecule. Figure 4 shows the energy profile for the direct hydrolysis of furan epoxide, which involved a higher activation barrier of 52.24 kcal/mol (**TS3**) without the involvement of heme-porphine. **TS3** involved the attack of the water molecule on C1 of the epoxide ring, leading to the formation of the covalent adduct **P3**. In **TS3**, C1---O(water) and C1---O(epoxide) distances were observed to be 1.68 and 2.40 Å, respectively. **P3** was observed to be stable by −22.32 kcal/mol (with respect to **P1**). The epoxide ring opening in **P1** was also studied in the presence of a heme-porphine center, as shown in Figure 4. The transition state structure $\mathbf{TS3_{heme}}$ was observed to be geometrically similar to **TS3**. The energy barrier was observed to be significantly reduced to 20.03 kcal/mol from 52.24 kcal/mol under the influence of heme-porphine. This decrease in the barrier might have arisen due to the oxygen (epoxide) coordination to the heme-iron, as evident by the decrease in Fe---O distance to 2.02 Å (in $\mathbf{TS3_{heme}}$) from 2.37 Å (in **PC**). The oxygen atom of the incoming water in $\mathbf{TS3_{heme}}$ attacks C1 and leads to epoxide ring opening, as indicated by d(C1---O_{water}) = 2.33 Å and d(C1---$O_{epoxide}$) = 2.17 Å. The C2−O distance was observed to be 1.38 Å, while the Fe−O−C2 angle was 120.9° in $\mathbf{TS3_{heme}}$. The ring-opened oxygen was found to be oriented in a perpendicular orientation to the heme-iron (the S−Fe−O bond angle is 173.9°, similar to that in the epoxide product (**PC**)). This indicates that even after the ring-opening reaction epoxide oxygen resides above the heme-iron owing to a strong electrostatic interaction (Fe---O = 2.02 Å). The Fe---O distance of 2.24 Å was observed in $\mathbf{P3_{heme}}$, stable by −23.39 kcal/mol. It was observed that the electrostatic interaction between heme-iron and oxygen remained throughout the metabolic pathway of the furan ring.

(ii). Carboxylate Ion Assisted Pathway for Hydrolysis. Since the energy barriers for the diol formation without (52.24 kcal/mol) and with (20.03 kcal/mol) the support of heme-porphine were very high, direct water attack may not take place inside the catalytic environment of CYPs. The active site cavity of a majority of CYP isoforms contains amino acids with the carboxylic acid side chain (such as glutamic acid); hence, the diol formation from **P1** may be assisted by this residue. A similar mechanism has been reported in epoxide hydrolase,[57] where the epoxide ring opening is assisted by amino acids with a carboxylic side chain.

The reaction path in this study was modeled using the nucleophilic acetate ion and proton donating acetic acid. This path involved two key steps, alkylation and hydrolysis, as shown in Figure 5. Initially, a reactant complex (Figure S3, see the Supporting Information) was formed, where the nucleophilic acetate showed H-bonding interactions with the hydrogen attached to C1 (2.03 Å) and hydrogen of the water molecule (1.78 Å). The other hydrogen of water was involved in an H-bonding interaction with acetic acid (H---O = 2.17 Å), while the hydrogen of acetic acid showed an H-bonding interaction with the epoxide oxygen (1.74 Å). In $\mathbf{TS_{alkylation}}$ (Figure 5), nucleophilic acetate is located at a distance of 2.40 Å from C1, and the C1---O(epoxide) distance increased to 1.47 Å. The $O_{acetate}$−C1−C2 bond angle was observed to be 101.6°, indicating favorable attack of the nucleophile in the epoxide ring-opening reactions, similar to those reported by Laitinen et al.[58] The proton transfer from acetic acid also takes place simultaneously, where the H---O(epoxide) distance was decreased to 1.47 Å, while the H---O(acetic acid) distance was elongated to 1.06 Å. The water molecule still showed an H-bonding interaction with acetate (H---O = 1.90 Å) and with acetic acid (1.91 Å). The alkylation step required a low barrier of 12.29 kcal/mol (Figure 4), leading to the formation of the stable covalent intermediate **CI** (ΔH = −24.76 kcal/mol). In **CI**, a covalent bond was formed between C1 and acetate, along with the protonation of the epoxide oxygen (1.01 Å).

The C1---O(acetic acid) distance was elongated to 2.46 Å, as compared to 1.06 Å in $\mathbf{TS_{alkylation}}$, indicating the donation of the proton to the epoxide oxygen. The covalent intermediate (**CI**) formed can undergo hydrolysis ($\mathbf{TS_{hydrolysis}}$) by the water molecule on its ester linkage. The water molecule attacks the carbonyl carbon atom, where the O_{water}---$C_{carbonyl}$ bond distance was observed to be 1.54 Å, while the hydrogen of water was observed to be located in proximity to the ester oxygen (2.07 Å). The O−C bond in the ester was found to become weaker in $\mathbf{TS_{hydrolysis}}$ (1.64 Å). The energy barrier for this step was calculated to be nearly barrierless (0.67 kcal/mol, not shown in Figure 4). This step leads to the formation of the complex of a highly stable (ΔH = −31.95 kcal/mol) diol product, **P3′** (Figure 4). This reaction path was also studied in the presence of the heme center, as shown in Figures 4 and 5. The covalent intermediate ($\mathbf{CI_{heme}}$) formed via $\mathbf{TS_{alkylation\text{-}heme}}$ (E_a = 10.73 kcal/mol) was observed to be less stable (ΔH = −15.98 kcal/mol) in comparison to **CI**. The covalent intermediate undergoes a similar barrierless hydrolysis step as discussed above to form the less stable product complex of vicinal diol ($\mathbf{P3'_{heme}}$, ΔH = −14.58 kcal/mol). The transition state was modeled on the basis of optimized geometries of similar reactions in epoxide hydrolases, reported by Hopmann et al.,[57] wherein similar bond distances were observed for the hydrolysis step. The optimized geometries in Figure 5 show the presence of heme iron and epoxide coordination at each step. It can also be observed that the epoxide oxygen is oriented perpendicularly to the heme-iron at each step, as indicated by S−Fe−O bond angles of 173.6−174.9° (Figure 5). This metal−oxygen coordination is the crucial factor, resulting in the decrease of the overall energy barrier on pathway B to 10.73 kcal/mol (Figure 4).

Overall, the reactions envisaged in pathway B can be possible with a barrier of ∼11 kcal/mol. This is possible only when an acidic center (glutamic acid, E308 in CYP3A4) comes close to the heme-substrate complex inside the cavity during induced fit. In CYP3A4, E308 is relatively far away; this decreases the possibility of diol formation during the catalysis by CYP3A4.

Pathway C: Epoxide Ring Opening by Nucleophilic Residues Leading to MBI of CYPs. CYPs have a few nucleophilic amino acid residues in their active site, which have been proposed to be responsible for the furan epoxide ring opening and covalent adduct formation, leading to MBI of CYPs (Scheme 2).[26−39] For this purpose, a systematic analysis of the crystal structures of various CYP isoforms (taken from the Protein Data Bank) was carried out. The analysis showed the presence of nucleophilic amino acids, serine and threonine, in the active site cavity of a majority of CYPs (CYP3A4, 2C9, and 2D6) within 5 Å from the heme-porphyrin unit (Figure S4, Supporting Information). Moreover, the threonine residue is present and conserved in most of the CYPs (with a different

dx.doi.org/10.1021/ic401907k | Inorg. Chem. 2013, 52, 13496−13508

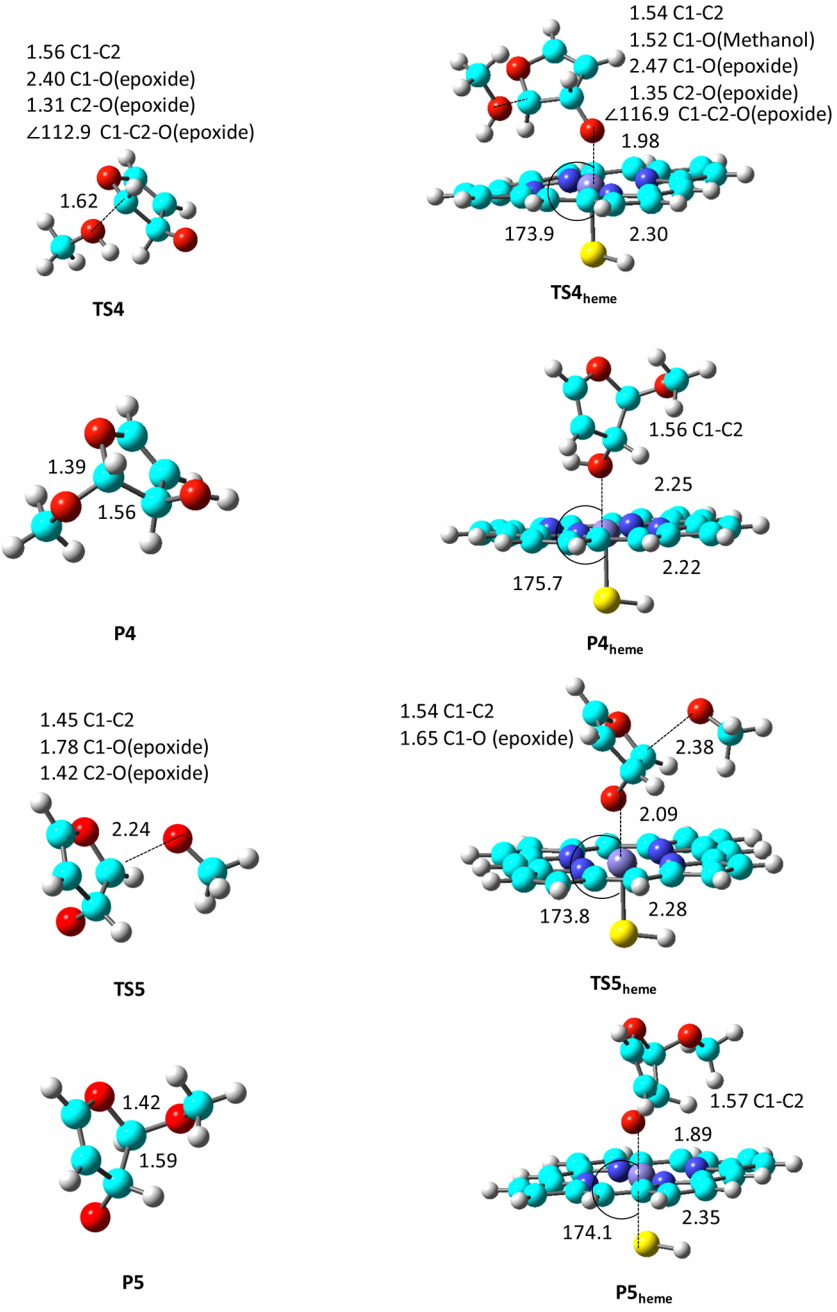

Figure 6. BS3-optimized geometries of the species involved in pathway C. Bond distances are given in Å and bond angles in deg. Color code: red, oxygen; sky blue, carbon; white, hydrogen; blue, nitrogen; gray, iron; yellow, sulfur.

residue number), and this residue is involved in the proton relay mechanism from the carboxylate side chain to the distal oxygen of **Cpd 0** (ferric-hydroperoxy species) leading to the formation of **Cpd I**.[58]

Hence, it can be ascertained that there is a higher probability of epoxide ring opening by nucleophilic serine/threonine present in the active site cavity of CYPs. These nucleophilic residues are active at the ROH group. The lone pair of electrons on the oxygen atom attacks the electrophilic C1 center of furan epoxide. Alternatively, the OH group may also get ionized first to RO^- with the help of basic residues (arginine) and subsequently the nucleophilic attack by the residue in anionic state can take place.

(i). Epoxide Ring Opening by Neutral Nucleophiles. The nucleophilic residues are modeled using oxygen-based methanol (MeOH) as the nucleophile. Figure 6 shows the 3D structures of the transition state (**TS4**) and product complex (**P4**) for the epoxide ring opening by MeOH. In **TS4**, the C1- - -O_{MeOH} distance was observed to be 1.62 Å, while the C1- - -$O_{epoxide}$ bond was elongated to 2.40 Å. The C1−C2 distance was marginally increased to 1.56 Å from 1.48 Å (furan epoxide). The C1−C2−O bond angle was observed to be 112.9°, confirming the epoxide ring-opening process. The energy barrier for this process has been estimated to be very high (40.27 kcal/mol, Figure 7). The ring opening results in the formation of the stable covalent adduct **P4** (ΔH = −22.26 kcal/mol), as evident from the C1- - -O distance (1.39 Å) and the transfer of a hydrogen atom from MeOH to the epoxide oxygen.

dx.doi.org/10.1021/ic401907k | *Inorg. Chem.* 2013, 52, 13496−13508

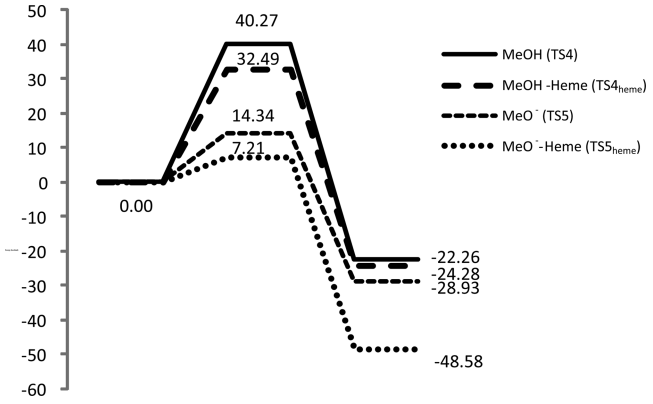

Figure 7. Potential energy surface on pathway C: nucleophilic epoxide ring opening with MeOH and MeO^- without and with heme-porphine (doublet spin state of **Cpd I**). Energies are given in kcal/mol, relative to furan epoxide.

Owing to the higher energy barrier observed in the above case, the ring-opening reaction was studied in the presence of the heme-porphine unit. $\mathbf{TS4_{heme}}$ shows the nucleophilic attack of methanol on the C1 center of furan epoxide, where the C1---O_{MeOH} distance as observed to be 1.52 Å, while the C1---$O_{epoxide}$ bond was elongated to 2.47 Å. During this ring-opening process, the epoxide oxygen was observed to be coordinated to heme-iron (1.98 Å) and oriented in a perpendicular orientation to the heme-porphine unit (the S–Fe–O angle is 173.9°). This process also required a high barrier of 32.49 kcal/mol, as shown in Figure 7. The formation of the stable adduct $\mathbf{P4_{heme}}$ was observed to be an exothermic process (−24.28 kcal/mol, with respect to **PC**). Thus, the barriers were observed to be higher with the model nucleophile MeOH in both instances (without and with heme-porphine). This prompted us to search for alternative pathways which could occur in the active site cavity of CYPs, leading to MBI.

(ii). Epoxide Ring Opening by Nucleophiles in Their Anionic State. A close examination of the crystal structures revealed the presence of a basic amino acid residue, arginine, in close proximity to the nucleophilic residue, serine (CYP3A4; Figure S4, Supporting Information); proton transfer from serine to arginine can generate the anionic state of serine. Thus, methoxide anion (MeO^-) was used as the model of anionic nucleophilic residues leading to the covalent modification of CYPs and, ultimately, MBI of CYPs. This pathway was also studied in the absence and presence of a heme-porphine unit. **TS5** and **P5** represent the transition state and product geometries in the absence of a heme-porphine unit (Figure 6). **TS5** was observed to be similar to **TS4**, with a C1---O_{MeO}^- distance of 2.24 Å and C1---$O_{epoxide}$ bond elongation to 1.78 Å. The energy barrier for this process has been estimated to be 14.34 kcal/mol. This reduction in the barrier was significant (~26 kcal/mol), in comparison with epoxide ring opening by the neutral nucleophile MeOH (40.27 kcal/mol). This reduction could be due to the strong nucleophilic character of MeO^- (global nucleophilicity, N = 5.78 eV) in comparison to MeOH (N = 2.00 eV). This process results in the formation of the covalent adduct **P5**, which is stable by 28.93 kcal/mol.

The process of epoxide ring opening by MeO^- in the presence of heme-porphine ($\mathbf{TS5_{heme}}$) gives a transition state

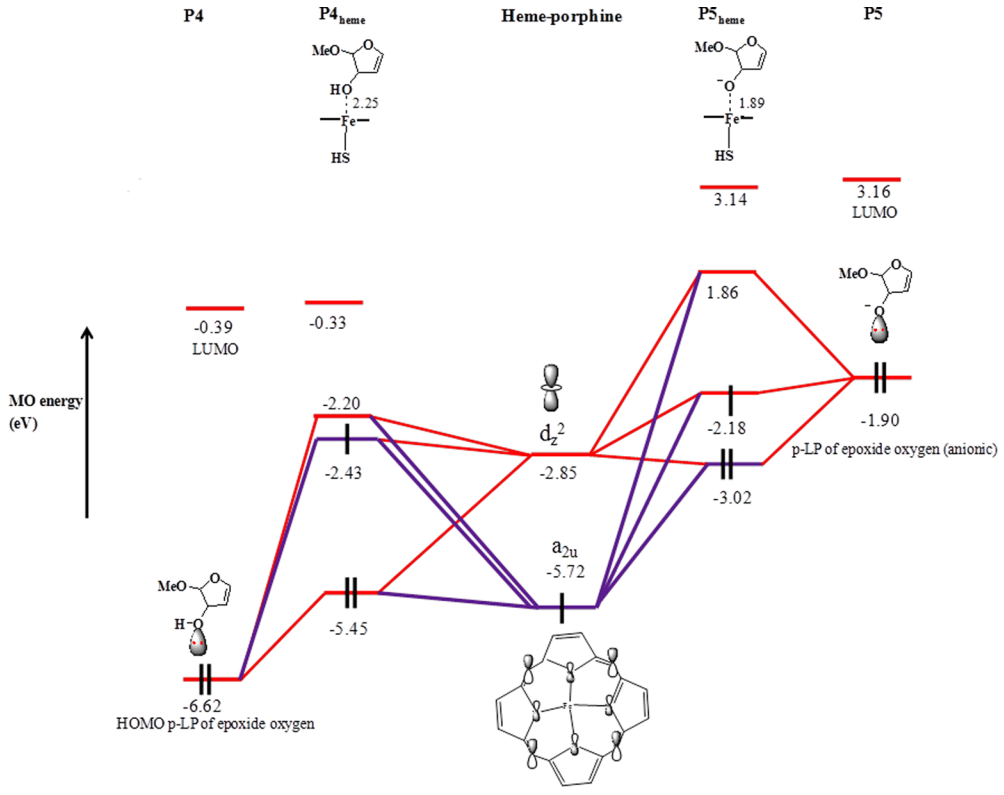

Figure 8. Orbital interaction diagram for the interactions between **P4** and heme-porphine leading to $\mathbf{P4_{heme}}$ (left-hand side) and interactions between **P5** and heme-porphine leading to $\mathbf{P5_{heme}}$ (right-hand side). The orbitals have been ordered according to the calculated eigenvalues in electronvolts (eV). The red line indicates an orbital interaction between p-LP (p-type lone pair) of epoxide oxygen and d_{z^2} of heme-iron, and the purple line indicates an orbital interaction between p-LP and a_{2u}.

dx.doi.org/10.1021/ic401907k | *Inorg. Chem.* 2013, 52, 13496–13508

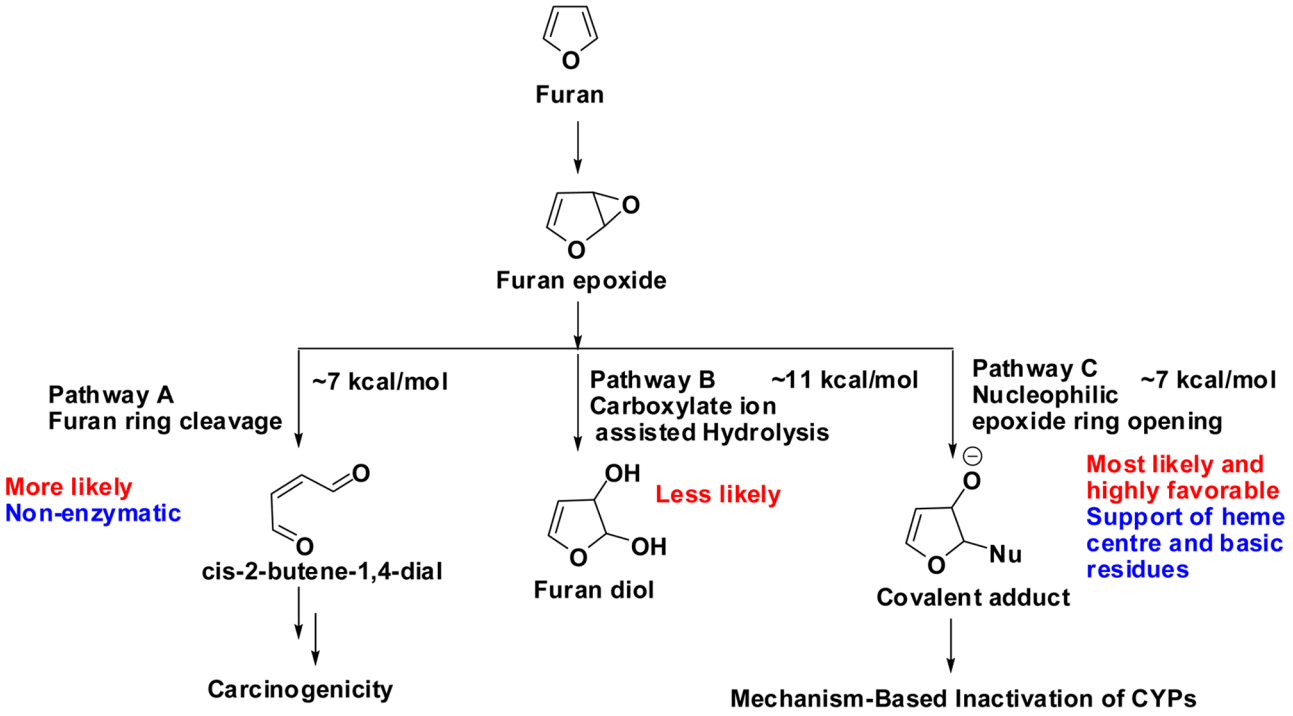

Figure 9. Schematic representation of furan epoxide reactivity, showing likely and less likely pathways.

and product complex geometries similar to those in the above case (**TS5**, Figure 6). $\mathbf{TS5}_{heme}$ shows the nucleophilic attack of MeO^- at the C1 center of furan epoxide, where the C1- - - $O_{MeO}{}^-$ distance was observed to be 2.38 Å, while the C1- - - $O_{epoxide}$ bond elongation was observed to be 1.65 Å. The C1−C2 distance marginally increased to 1.54 Å from 1.48 Å in the furan epoxide product (**PC**).

The ring-opened epoxide oxygen lies at a distance of 2.09 Å from heme-iron, in a perpendicular orientation (S−Fe−O bond angle, 173.8°). The energy barrier for ring opening by MeO^- in the presence of heme-porphine decreased considerably to 7.21 kcal/mol (Figure 7). This decrease of ∼7 kcal/mol indicates the significant role played by the metal center (heme-iron) which is in coordination with the epoxide oxygen, along with the stronger nucleophilicity of MeO^- as discussed above. $\mathbf{P5}_{heme}$ represents the covalent adduct of furan epoxide with MeO^- in the presence of heme-porphine, where the C1−C2 bond distance was observed to be 1.57 Å, and a strong coordinating interaction between epoxide oxygen and heme-iron (1.89 Å) was observed. The S−Fe−O bond angle of 174.1° further highlights this coordination. Owing to this stronger interaction, $\mathbf{P5}_{heme}$ was observed to be a highly stable (48.58 kcal/mol, with respect to **PC**) covalent adduct capable of inactivating CYPs, leading to MBI. In an overall reaction starting from furan, the covalent adducts are observed to be highly stable ($\mathbf{P4}_{heme}$, −45.91 kcal/mol; $\mathbf{P5}_{heme}$, −70.22 kcal/mol), thereby confirming them as inactivator (inhibitor) complexes of CYPs, similar to so-called suicidal complexes of terminal olefins with heme-porphyrin in CYPs.[59]

(iii). Molecular Orbital (MO) Analysis of Inactivator Complexes $P4_{heme}$ *and* $P5_{heme}$. A detailed analysis for the electronic structure of the inactivator complexes $\mathbf{P4}_{heme}$ (−24.28 kcal/mol) and $\mathbf{P5}_{heme}$ (−48.58 kcal/mol) was carried out using the fragment molecular orbital approach (Figure 8). The HOMOs of both ligands participate in the interaction, whereas the LUMOs of the ligands remain unperturbed.

The energy of the HOMO in **P5** (−1.90 eV) is much higher as compared to the energy of the HOMO in **P4** (−6.62 eV). The interaction with the heme-porphine center (d_{z^2} orbital) stabilizes the electrons in **P5**, whereas it destabilizes the electrons in **P4**. Thus, $\mathbf{P5}_{heme}$ formation involves stabilizing forces, whereas $\mathbf{P4}_{heme}$ formation involves destabilizing forces. This is reflected in a lower barrier for the formation of $\mathbf{P5}_{heme}$ (Figure 7). On the other hand, molecular orbitals of $\mathbf{P5}_{heme}$ are much higher in energy in comparison to the molecular orbitals of $\mathbf{P4}_{heme}$. This would prompt $\mathbf{P5}_{heme}$ to pick up a proton and form $\mathbf{P4}_{heme}$, eventually breaking the Fe- - -O bond and leaving the heme-porphine center free. Because of the covalent adduct thus formed between serine and furan epoxide, the catalytic activity of CYPs gets blocked.

The detailed study of all the reaction pathways reported in this article emphasized that furan epoxide can undergo nonenzymatic furan ring cleavage (pathway A) on a more likely pathway, which may not lead to MBI of CYPs. Pathway B involving uncatalyzed or acid-assisted hydrolysis does not lead to MBI of CYPs and involves an overall barrier of ∼11 kcal mol. Pathway C involving nucleophilic epoxide ring opening via an overall barrier of ∼7 kcal/mol and with the support of heme center and basic amino acid residues is the most likely and favorable reaction pathway leading to MBI of CYPs (Figure 9).

■ CONCLUSIONS

The mechanistic details for the formation of reactive epoxide intermediates from compounds containing a furan ring, leading to the covalent modification of CYPs and MBI, were explored using quantum chemical methods. A DFT study was carried out to elucidate the mechanistic details for the epoxidation of the furan ring with **Cpd I**. The activation barrier for the transition of the furan ring to furan epoxide was observed to be 12.33 kcal/mol. This implied that the epoxidation of furan by CYPs directly involving the heme-porphine center is a highly feasible process. The furan epoxide metabolite can follow three

dx.doi.org/10.1021/ic401907k | *Inorg. Chem.* 2013, 52, 13496−13508

pathways leading to different products. The furan ring cleavage (pathway A) leading to the formation of a carcinogenic dialdehyde intermediate is a highly probable process requiring only ∼7 kcal/mol. The hydrolysis (pathway B) required the assistance of the carboxylate anion and the heme center, with an overall barrier of ∼11 kcal/mol. This pathway was favored in the presence of water molecule(s) in the active site cavity of CYPs. On the other hand, the possibility of MBI via a nucleophilic ring-opening reaction required ∼7 kcal/mol and is largely facilitated by the initial activation of nucleophilic serine/threonine and the support of the heme center. Hence, it can be established that the three different reactions occurring on the furan epoxide are highly competitive.

The molecular level insights gained from this quantum chemical study provide clues, for the first time, regarding the three competitive reactions of the epoxide metabolite and answer several questions about the pathway of furan metabolism leading to the covalent modification of CYPs. The initial epoxidation of furan by CYPs is the rate-determining step on the whole reaction pathway leading to MBI.

The key factors which facilitate MBI by the reactive epoxide metabolite are (i) the availability of the nucleophilic amino acid residue(s) (serine/threonine) in the vicinity of the epoxide ring, (ii) initial activation of these residues by nearby basic amino acids (such as arginine), (iii) the absence of water molecule(s) in the active site cavity of CYPs to avoid competitive hydrolysis reactions, (iv) participation of a heme center at every step on the metabolic pathway of the furan ring. The molecular level details of the mechanism of MBI by the reactive epoxide metabolite provide information on the likely liabilities and help in dealing with the MBI of CYPs in early drug discovery. This study provides the atomic level and energetic details for the reaction pathway leading to MBI by the epoxide metabolite, which would aid the experimental and drug metabolism scientists in minimizing the likelihood of CYP inactivation. Such an analysis is a significant step for creating an opportunity to consider carrying out synthetic modifications on lead molecules to eliminate the tendency to generate such undesirable, reactive, and toxic metabolites.

■ ASSOCIATED CONTENT

Supporting Information

Standard equations for calculating nucleophilicity and electrophilicty parameters (S1), Fukui, charge, electrophilicity, and nucleophilicity parameter analysis (Table S1 and Table S2), AIM analysis of *cis*-2-butene-1,4-dial (Figure S1), crystal structures showing water molecules in the active site of CYPs (Figure S2), optimized structures of reactant complexes (Figure S3), crystal structures of various CYP isoforms showing the presence of nucleophilic (serine/threonine) and basic residues (arginine) (Figure S4), spin density and NBO analysis (Table S3 and Table S4), absolute energies of the optimized geometries at all the basis sets (Table S5), and *XYZ* coordinates of key geometries (S2). This material is available free of charge via the Internet at http://pubs.acs.org.

■ AUTHOR INFORMATION

Corresponding Author

*E-mail for P.V.B.: pvbharatam@niper.ac.in.

Notes

The authors declare no competing financial interest.

■ ACKNOWLEDGMENTS

N.T. thanks the Department of Science and Technology (DST) for a DST-INSPIRE Ph.D. Fellowship. The authors are grateful to the Department of Biotechnology (DBT), New Delhi, India, for providing financial assistance.

■ REFERENCES

(1) Seth, K.; Roy, S. R.; Pipaliya, B. V.; Chakraborti, A. K. *Chem. Commun.* **2013**, *49*, 5886−5888.
(2) McEwan, K. A.; Slavin, S.; Tunnah, E.; Haddleton, D. M. *Polym. Chem.* **2013**, *4*, 2608−2614.
(3) Ji, L.; Zhang, D.-F.; Zhao, Q.; Hu, S.-M.; Qian, C.; Chen, X-.Z. *Tetrahedron* **2013**, *69*, 7031−7037.
(4) Kotani, S.; Furusho, H.; Sugiura, M.; Nakajima, M. *Tetrahedron* **2013**, *69*, 3075−3081.
(5) Wang, L.; Li, G.-F.; Liu, M.; Deng, D.; Pei, Y.; Wang, X. *Inorg. Chem. Commun.* **2013**, *32*, 192−194.
(6) de Rezende, L. C. D.; Fumagalli, F.; Bortolin, M. S.; de Oliveira, M. G.; de Paula, M. H.; de A. Neto, V. F.; da S. Emery, F. *Bioorg. Med. Chem. Lett.* **2013**, DOI: 10.1016/j.bmcl.2013.06.033.
(7) Krake, S. H.; Bergmeier, S. C. *Tetrahedron* **2010**, *66*, 7337−7360.
(8) Nam, W.; Kim, H. J.; Kim, S. H.; Ho, R. Y.; Valentine, J. S. *Inorg. Chem.* **1996**, *35*, 1045−1049.
(9) Nam, W.; Lee, H. J.; Oha, S.-Y.; Kim, C.; Jang, H. G. *J. Inorg. Biochem.* **2000**, *80*, 219−225.
(10) Song, W. J.; Ryu, Y. O.; Song, R.; Nam, W. *J. Biol. Inorg. Chem.* **2005**, *10*, 294−304.
(11) (a) Yin, G.; Buchalova, M.; Danby, A. M.; Perkins, C. M.; Kitko, D.; Carter, J. D.; Scheper, W. M.; Busch, D. H. *J. Am. Chem. Soc.* **2005**, *127*, 17170−17171. (b) Yin, G.; Buchalova, M.; Danby, A. M.; Perkins, C. M.; Kitko, D.; Carter, J. D.; Scheper, W. M.; Busch, D. H. *Inorg. Chem.* **2006**, *45*, 3467−3474.
(12) Bautz, J.; Comba, P.; de Laorden, C. L.; Menzel, M.; Rajaraman, G. *Angew. Chem., Int. Ed.* **2007**, *46*, 8067−8070.
(13) Franke, A.; Fertinger, C.; van Eldik, R. *Angew. Chem., Int. Ed.* **2008**, *47*, 5238−5242.
(14) Lee, S. H.; Lee, E. Y.; Yoo, D.-W.; Hong, S. J.; Lee, J. H.; Kwak, H.; Lee, Y. M.; Kim, J.; Kim, C.; Lee, J.-K. *New J. Chem.* **2007**, *31*, 1579−1582.
(15) Houghton, R. P.; Rice, C. R. *J. Chem. Soc., Chem. Commun.* **1995**, 2265−2266.
(16) Abashkin, Y. G.; Collins, J. R.; Burt, S. K. *Inorg. Chem.* **2001**, *40*, 4040−4048.
(17) Comba, P.; Rajaraman, G. *Inorg. Chem.* **2008**, *47*, 78−93.
(18) Valentin, C. D.; Gisdakis, P.; Yudanov, I. V.; Rösch, N. *J. Org. Chem.* **2000**, *65*, 2996−3004.
(19) Ishikawa, A.; Sakaki, S. *J. Phys. Chem. A* **2011**, *115*, 4774−4785.
(20) Shaik, S.; de Visser, S. P.; Ogliaro, F.; Schwarz, H.; Schröder, D. *Curr. Opin. Chem. Biol.* **2002**, *6*, 556−567.
(21) (a) Kumar, D.; Karamzadeh, B.; Sastry, G. N.; de Visser, S. P. *J. Am. Chem. Soc.* **2010**, *132*, 7656−7667. (b) Kumar, D.; Latifi, R.; Kumar, S.; Rybak-Akimova, E. V.; Sainna, M. A.; de Visser, S. P. *Inorg. Chem.* **2013**, *52*, 7968−7979. (c) Kumar, D.; Tahsini, L.; de Visser, S. P.; Kang, H. Y.; Kim, S. J.; Nam, W. *J. Phys. Chem. A* **2009**, *113*, 11713−11722.
(22) (a) de Visser, S. P.; Ogliaro, F.; Sharma, P. K.; Shaik, S. *J. Am. Chem. Soc.* **2002**, *124*, 11809−11826. (b) de Visser, S. P.; Ogliaro, F.; Sharma, P. K.; Shaik, S. *Angew. Chem.* **2002**, *114*, 2027−2031. (c) de Visser, S. P.; Ogliaro, F.; Harris, F.; Shaik, S. *J. Am. Chem. Soc.* **2001**, *123*, 3037−3047.
(23) Lonsdale, R.; Harvey, J. N.; Mulholland, A. J. *J. Phys. Chem. B* **2010**, *114*, 1156−1162.
(24) Van Horn, W. D. *Crit. Rev. Biochem. Mol. Biol.* **2013**, *48*, 357−372.
(25) (a) Archelas, A.; Furstoss, R. *Curr. Opin. Chem. Biol.* **2001**, *5*, 112−119. (b) Schmelzer, K. R.; Kubala, L.; Newman, J. W.; Kim, I.-H.; Eiserich, J. P.; Hammock, B. D. *Proc. Natl. Acad. Sci. U.S.A.* **2005**, *102*,

9722−9777. (c) Imig, J. D.; Hammock, B. D. *Nat. Rev. Drug Discov.* **2009**, *8*, 794−805.
(26) Sesardic, D.; Boobis, A. R.; Murray, B. P.; Murray, S.; Segura, J.; De La Torre, R.; Davies, D. S. *Br. J. Clin. Pharmacol.* **1990**, *29*, 651−663.
(27) Kunze, K. L.; Trager, W. F. *Chem. Res. Toxicol.* **1993**, *6*, 646−656.
(28) Chiba, M.; Nishime, J. A.; Lin, J. H. *J. Pharmacol. Exp.* **1995**, *275*, 1527−1534.
(29) Lightning, L. K.; Jones, J. P.; Friedberg, T.; Pritchard, M. P.; Shou, M.; Rushmore, T. H.; Trager, W. F. *Biochemistry* **2000**, *39*, 4276−4287.
(30) Koenigs, L. L.; Peter, R. M.; Thompson, S. J.; Rettie, A. E.; Trager, W. F. *Drug. Metab. Dispos.* **1997**, *25*, 1407−1415.
(31) Tinel, M.; Belghiti, J.; Descatoire, V.; Amouyal, G.; Letteron, P.; Geneve, J.; Larrey, D.; Pessayre, D. *Biochem. Pharmacol.* **1987**, *36*, 951−955.
(32) Schmiedlin-Ren, P.; Edwards, D. J.; Fitzsimmons, M. E.; He, K.; Lown, K. S.; Woster, P. M.; Rahman, A.; Thummel, K. E.; Fisher, J. M.; Hollenberg, P. F.; Watkins, P. B. *Drug Metab. Dispos.* **1997**, *25*, 1228−1233.
(33) Alvarez-Diez, T. M.; Zheng, J. *Chem. Res. Toxicol.* **2004**, *17*, 150−157.
(34) Edwards, D. J.; Bellevue, F. H.; Woster, P. M. *Drug Metab. Dispos.* **1996**, *24*, 128−129.
(35) He, K.; Iyer, K. R.; Hayes, R. N.; Sinz, M. W.; Woolf, T. F.; Hollenberg, P. F. *Chem. Res. Toxicol.* **1998**, *11*, 252−259.
(36) Girennavar, B.; Poulose, S. M.; Jayaprakasha, G. K.; Bhat, N. G.; Patil, B. S. *Bioorg. Med. Chem.* **2006**, *14*, 2606−2612.
(37) Guo, L. Q.; Fukuda, K.; Ohta, T.; Yamazoe, Y. *Drug Metab. Dispos.* **2000**, *28*, 766−771.
(38) Ueng, Y. F.; Kuwabara, T.; Chun, Y. J.; Guengerich, F. P. *Biochemistry* **1997**, *36*, 370−381.
(39) (a) Orr, S. T. M.; Ripp, S. L.; Ballard, T. E.; Henderson, J. L.; Scott, D. O.; Obach, R. S.; Sun, H.; Kalgutkar, A. S. *J. Med. Chem.* **2012**, *55*, 4896−4933. (b) Stepan, A. F.; Mascitti, V.; Beaumont, K.; Kalgutkar, A. S. *Med. Chem. Commun.* **2013**, *4*, 631−652. (c) Kalgutkar, A. S.; Obach, R. S.; Maurer, T. S. *Curr. Drug Metab.* **2007**, *8*, 407−447. (d) Kent, U. M.; Jushchyshyn, M. I.; Hollenberg, P. F. *Curr. Drug Metab.* **2001**, *2*, 215−243. (e) Fontana, E.; Dansette, P. M.; Poli, S. M. *Curr. Drug Metab.* **2005**, *6*, 413−454. (f) Hollenberg, P. F.; Kent, U. M.; Bumpus, N. N. *Chem. Res. Toxicol.* **2008**, *21*, 189−205. (g) Kamel, A.; Harriman, S. *Drug Discov. Today Technol.* **2013**, *10*, 177−189. (h) Guengerich, F. P. *Chem. Res. Toxicol.* **2008**, *2*, 70−83. (i) Sun, H.; Scott, D. O. *Chem. Biol. Drug Des.* **2010**, *75*, 3−17.
(40) (a) Taxak, N.; Desai, P. V.; Patel, B.; Mohutsky, M.; Klimkowski, V. J.; Gombar, V.; Bharatam, P. V. *J. Comput. Chem.* **2012**, *33*, 1740−1747. (b) Taxak, N.; Patel, B.; Bharatam, P. V. *Inorg. Chem.* **2013**, *52*, 5097−5109.
(41) (a) Hirao, H.; Chuanprasit, P.; Cheong, Y. Y.; Wang, X. *Chem. Eur. J.* **2013**, *19*, 7361−7369. (b) Hirao, H.; Cheong, Z. H.; Wang, X. *J. Phys. Chem. B* **2012**, *116*, 7787−7794.
(42) Parr, R. G.; Yang, W. *Density Functional Theory of Atoms and Molecules*: Oxford University Press: New York, 1989; pp 1−325.
(43) Frisch, M. J.; Trucks, G. W.; Schlegel, H. B.; Scuseria, G. E.; Robb, M. A.; Cheeseman, J. R.; Scalmani, G.; Barone, V.; Mennucci, B.; Petersson, G. A.; Nakatsuji, H.; Caricato, M.; Li, X.; Hratchian, H. P.; Izmaylov, A. F.; Bloino, J.; Zheng, G.; Sonnenberg, J. L.; Hada, M.; Ehara, M.; Toyota, K.; Fukuda, R.; Hasegawa, J.; Ishida, M.; Nakajima, T.; Honda, Y.; Kitao, O.; Nakai, H.; Vreven, T.; Montgomery, J. A., Jr.; Peralta, J. E.; Ogliaro, F.; Bearpark, M.; Heyd, J. J.; Brothers, E.; Kudin, K. N.; Staroverov, V. N.; Kobayashi, R.; Normand, J.; Raghavachari, K.; Rendell, A.; Burant, J. C.; Iyengar, S. S.; Tomasi, J.; Cossi, M.; Rega, N.; Millam, J. M.; Klene, M.; Knox, J. E.; Cross, J. B.; Bakken, V.; Adamo, C.; Jaramillo, J.; Gomperts, R.; Stratmann, R. E.; Yazyev, O.; Austin, A. J.; Cammi, R.; Pomelli, C.; Ochterski, J. W.; Martin, R. L.; Morokuma, K.; Zakrzewski, V. G.; Voth, G. A.; Salvador, P.; Dannenberg, J. J.; Dapprich, S.; Daniels, A. D.; Farkas, Ö.; Foresman, J. B.; Ortiz, J. V.; Cioslowski, J.; Fox, D. J. *Gaussian 03, revision C.02*; Gaussian, Inc., Wallingford, CT, 2004.
(44) (a) Foresman, J. B.; Frisch, A. E. *Exploring Chemistry with Electronic Structure Methods*; Gaussian, Inc.: Pittsburgh, PA, 1995. (b) Hehre, W. J.; Radom, L.; Schleyer, P. v. R.; Pople, J. A. *Ab Initio Molecular Orbital Theory*; Wiley: New York, 1986. (c) Hay, P. J.; Wadt, W. R. *J. Chem. Phys.* **1985**, *82*, 270−283.
(45) (a) Becke, A. D. *J. Chem. Phys.* **1993**, *98*, 5648−5652. (b) Becke, A. D. *J. Chem. Phys.* **1993**, *98*, 1372−1377. (c) Lee, C. T.; Yang, W. T.; Parr, R. G. *Phys. Rev. B: Condens. Matter Mater. Phys.* **1988**, *37*, 785−789.
(46) Ochterski, J. W. Gaussian, Inc.; http://www.Gaussian.com/g_white-pap/thermo.htm.
(47) Scott, A. P.; Radom, L. *J. Phys. Chem.* **1996**, *100*, 16502−16513.
(48) (a) Taxak, N.; Dixit, V. A.; Bharatam, P. V. *J. Phys. Chem. A* **2012**, *116*, 10441−10450. (b) Taxak, N.; Prasad, K. C.; Bharatam, P. V. *Comput. Theor. Chem.* **2013**, *1007*, 48−56. (c) de Visser, S. P. *J. Am. Chem. Soc.* **2010**, *132*, 1087−1097. (d) Rydberg, P. *J. Chem. Theory Comput.* **2012**, *8*, 2706−2714. (e) Rydberg, P.; Olsen, L. *J. Chem. Theory Comput.* **2011**, *7*, 3399−3404. (f) Shaik, S.; Cohen, S.; Wang, Y.; Chen, H.; Kumar, D.; Thiel, W. *Chem. Rev.* **2010**, *110*, 949−1017. (g) Porros, C. S.; Sutcliffe, M. J.; de Visser, S. P. *J. Phys. Chem. A* **2009**, *113*, 11635−11642. (h) Shaik, S.; Hirao, H.; Kumar, D. *Acc. Chem. Res.* **2007**, *40*, 532−542. (i) Kumar, D.; Thiel, W.; de Visser, S. P. *J. Am. Chem. Soc.* **2011**, *133*, 3869−3882. (j) Kumar, D.; de Visser, S. P.; Sharma, P. K.; Hirao, H.; Shaik, S. *Biochemistry* **2005**, *44*, 8148−8158. (k) Tahsini, L.; Bagherzadeh, M.; Nam, W.; de Visser, S. P. *Inorg. Chem.* **2009**, *48*, 6661−6669.
(49) (a) Schaefer, A.; Huber, C.; Ahlrichs, R. *J. Chem. Phys.* **1994**, *100*, 5829−5835. (b) Schaefer, A.; Horn, H.; Ahlrichs, R. *J. Chem. Phys.* **1992**, *97*, 2571−2577.
(50) (a) Tomasi, J.; Mennucci, B.; Cancès, E. *J. Mol. Struct. (THEOCHEM)* **1999**, *464*, 211. (b) Cancès, M. T.; Mennucci, B.; Tomasi, J. *J. Chem. Phys.* **1997**, *107*, 3032−3041. (c) Mennucci, B.; Cancès, E.; Tomasi, J. *J. Phys. Chem. B* **1997**, *101*, 10506−10517.
(51) Reed, A. E.; Weinstock, R. B.; Weinhold, F. *J. Chem. Phys.* **1985**, *83*, 735−746.
(52) Bader, R. F. W. *Atoms in Molecules: A Quantum Theory*; Clarendon Press: Oxford, U.K., 1990.
(53) (a) Chattaraj, P. K.; Sarkar, U.; Roy, D. R. *Chem. Rev.* **2006**, *106*, 2065−2091. (b) Chattaraj, P. K.; Chakraborty, A.; Giri, S. *J. Phys. Chem. A* **2009**, *113*, 10068−10074.
(54) (a) Fukui, K. *Science* **1982**, *218*, 747−754. (b) Fukui, K.; Yonezawa, T.; Shingu, H. *J. Chem. Phys.* **1952**, *20*, 722−725.
(55) (a) Peterson, L. A.; Phillips, M. B.; Lu, D.; Sullivan, M. M. *Chem. Res. Toxicol.* **2011**, *24*, 1924−1936. (b) Byrns, M. C.; Vu, C. C.; Neidigh, J. W.; Abad, J.-L.; Jones, R. A.; Peterson, L. A. *Chem. Res. Toxicol.* **2006**, *19*, 414−420.
(56) Peterson, L. A. *Chem. Res. Toxicol.* **2013**, *26*, 6−25.
(57) (a) Hopmann, K. H.; Himo, F. *Chem. Eur. J.* **2006**, *12*, 6898−6909. (b) Hopmann, K. H.; Hallberg, B. M.; Himo, F. *J. Am. Chem. Soc.* **2005**, *127*, 14339−14347.
(58) Laitinen, T.; Rouvinen, J.; Peräkylä, M. *J. Org. Chem.* **1998**, *63*, 8157−8162.
(59) (a) Denisov, I. G.; Makris, T. M.; Sligar, S. G.; Schlichting, I. *Chem. Rev.* **2005**, *105*, 2253−2277. (b) Meunier, B.; de Visser, S. P.; Shaik, S. *Chem. Rev.* **2004**, *104*, 3947−3980. (c) Shaik, S.; Kumar, D.; de Visser, S. P.; Altun, A.; Thiel, W. *Chem. Rev.* **2005**, *105*, 2279−2328.
(60) de Visser, S. P.; Ogliaro, F.; Shaik, S. *Angew. Chem., Int. Ed.* **2001**, *40*, 2871−2874.